Article

The Role of Cloud in the Transportation of Dust into Basin Area: A Case Study in Sichuan Basin, Southwesten China

Yuelin Liu [1], Guangming Shi [1,2,*], Yunsong Du [1,3], Mengyao Lyu [4,5], Wei Zhang [3] and Fumo Yang [1,2]

[1] Department of Environmental Science and Engineering, Sichuan University, Chengdu 610065, China
[2] National Engineering Research Center on Flue Gas Desulfurization, Chengdu 610065, China
[3] Sichuan Eco-environment Monitoring Station, Chengdu 610095, China
[4] National Meteorological Centre, Beijing 100080, China
[5] Key Laboratory of Transportation Meteorology of China Meteorological Administration (CMA), Nanjing Joint Institute for Atmospheric Sciences, Nanjing 211512, China
[*] Correspondence: shigm@scu.edu.cn

Abstract: The existing knowledge illustrated the role of surrounding mountains in the transportation of dust into a basin, including the blocking of low-layer dust and the allowance of elevated dust intrusion. Taking the Sichuan Basin in southwestern China as an example, we found the impact of clouds on the transportation process of dust in the basin area. If there were low-level clouds on the basin edges, the dust particles could not penetrate the cloud layers, but settled down from upper air into the basin in the cloudless regions. They could be transported beneath clouds in the basin. Considering that the upslope airflow accompanied by dust transportation was conducive to the low-level clouds on the basin edge, this mechanism further reduced the dust intrusion besides the shelter of the surrounding mountains.

Keywords: dust transportation; cloud blocking; Sichuan Basin

1. Introduction

Mineral dust is one of the important components of atmospheric aerosol and plays a major role in the climate [1–3], air quality [4–6], and human health [7,8]. Dust particles can be lifted by strong winds and travel long distances, influencing a wide area. It not only can alter cloud properties [9,10] and change the Earth's radiation [11]. Moreover, dust particles can be carried to downwind area and impact the characteristics of local atmospheric chemistry [12,13].

The Sichuan Basin (SB) is located in the eastern leeward region of the Qinghai-Tibet Plateau and surrounded by high-altitude mountains as shown in Figure 1. Moreover, Sichuan Basin is one of the most heavily polluted regions in China and its air quality is a research hotspot. Previous studies suggest that SB could also be influenced by long-range transported dust [14–18] and that the PM_{10} concentration more than 1000 µg/m^3 was recorded when dust passed through the basin [14]. Some of these studies considered that the mountains make a great difference to the transportation of dust into the basin [14,15]. On one hand, the relatively lower altitude of the northern mountains allowed the intrusion of dust, and the dust air masses broke into the basin in the northeast direction after being elevated, and traveled around the mountains on the west side of the basin. On the other hand, the northern and western mountains sheltered the Sichuan Basin from more dust intrusions. Under this unique deep-basin topography, the convergence of northern and southern westerlies around the Tibetan Plateau leads to frequent cloud cover over the basin [19] and the climate cloud cover fraction is over 80% [20,21]. However, there still is no attention paid to the role of clouds in the transportation of dust into basin area. In this study, we explored the impact of clouds on the transportation of dust into the basin because it could provide insights into transportation mechanisms of dust in a basin area.
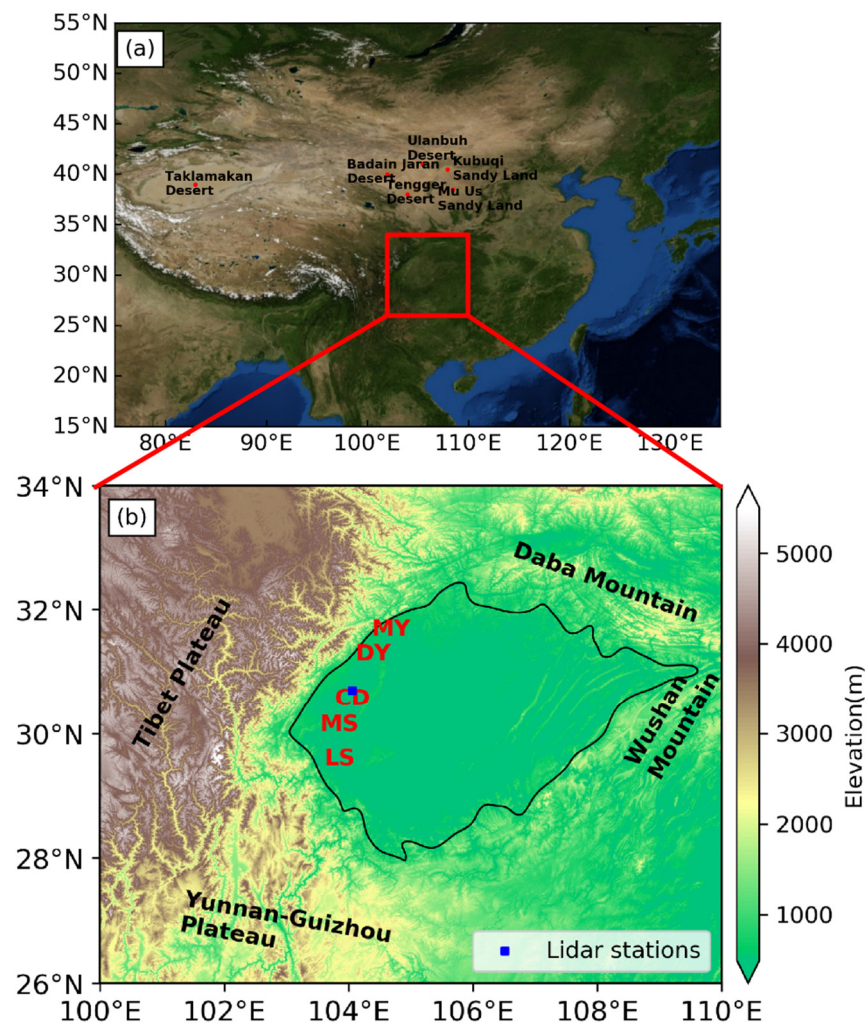
Figure 1. The geographical location (**a**) and topography (**b**) of the study area. The blue square marks the ground lidar station. The black line gives the isoline with a topographic elevation of 750 m above sea level. The city acronyms of MY, DY, CD, MS, and LS represent Mianyang, Deyang, Chengdu, Meishan, and Leshan, respectively.

2. Materials and Methods

2.1. Ground Lidar Observations

The ground lidar measurements were conducted during the dust event from 19 March to 26 March 2021. The lidar station was located in the urban area of Chengdu (104.06° E, 30.70° N) as shown in Figure 1b. The lidar was manufactured by EVERISE TECHNOLOGY LTD. and equipped with a Mie-scattering polarized system at a wavelength of 532 nm. The temporal and vertical resolutions of the retrieved data were 5 min and 15 m, respectively. The retrieved extinction coefficients and depolarization ratios were used in this study to identify and investigate the vertical feature of transported dust. The depolarization ratio is related to the shape of the atmospheric particle and is widely used to distinguish smoke, dust, and clouds [13,22]. According to previous studies, the presence of dust particles is approved by the depolarization ratio greater than 0.1 at 532 nm [13,23,24]. Cloud layers are identified by a relatively smaller depolarization ratio [25], which is usually lower than 0.09. Moreover, the extinction coefficient of cloud is relatively higher and the vertical gradient of extinction coefficient cloud top is sharp [26,27].

2.2. Satellite Observations

The observations from Cloud-Aerosol Lidar with Orthogonal Polarization (CALIOP), a space-based lidar onboard Cloud-Aerosol Lidar and Infrared Pathfinder Satellite Observation (CALIPSO) satellite, were retrieved to analyze Vertical Feature Mask (VFM) product (Version 4.20) with horizontal resolution of 5 km. It was used to identify the vertical structure of aerosols and clouds [28,29]. In addition, the Level-2 cloud products (MOD06_L2 and MYD06_L2) of Moderate-Resolution Imaging Spectroradiometer (MODIS) onboard Terra and Aqua satellites were used to analyze the distribution of cloud fractions [30,31].

2.3. Near Surface Meteorological and Air Quality Data

The fifth generation ECMWF reanalysis for the global climate and weather (ERA5) was used to retrieve meteorological parameters, including zonal and meridional winds, geopotential heights, and cloud cover fractions from 1000 hPa to 500 hPa [32]. The horizontal and temporal resolutions were $0.25° \times 0.25°$ and 1 h, respectively. The surface meteorological observations at Chengdu retrieved from China Meteorological Data Network (http://data.cma.cn/, accessed on 29 March 2021) were used, including wind speed, wind direction, cloud height, and cloud cover frication. Furthermore, the hourly PM_{10} and $PM_{2.5}$ concentrations were retrieved from the publishing website of China National Environmental Monitoring Center (https://air.cnemc.cn:18007/, accessed on 29 March 2021).

2.4. Backward Trajectories Simulation

The back trajectories, which were generated by the NOAA Hybrid Single-Particle Lagrangian Integrated Trajectory (HYSPLIT) model [33] and driven by the GDAS (Global Data Analysis System) meteorological data with spatial resolution of $1° \times 1°$, were used to trace the transportation path of dust.

3. Results

3.1. Overview of a Dust Event during March 2021

A strong sandstorm occurred during 14–18 March 2021 originating from the desert area of Mongolia and northwestern China. East Asia was influenced by the blowing sand in the following several days [34,35]. Affected by this strong sandstorm, the Sichuan Basin confronted severe dust pollution starting on 19 March 2021 (Figure S1). The air mass trajectory presented in Figure 2a revealed that this dust pollution could be ascribed to the transportation of desert area of northern China. The orientation of dust intrusion followed the air mass trajectories in the starting stage, but deviated in the following days. As shown in Figure 2b, the concentrations of coarse particles ($PM_{10}-PM_{2.5}$) increased sequentially from Mianyang in the north to Leshan in the South since the afternoon of 19 March. However, on 24 March, the influence of dust was obvious in the south part of the basin, but started dissipating in the north, as presented in Figure 2d. The causes for this difference were not apparently acquirable to our knowledge. Hence, taking this case as an example, we investigated the influencing factors of dust transportation in Sichuan Basin.
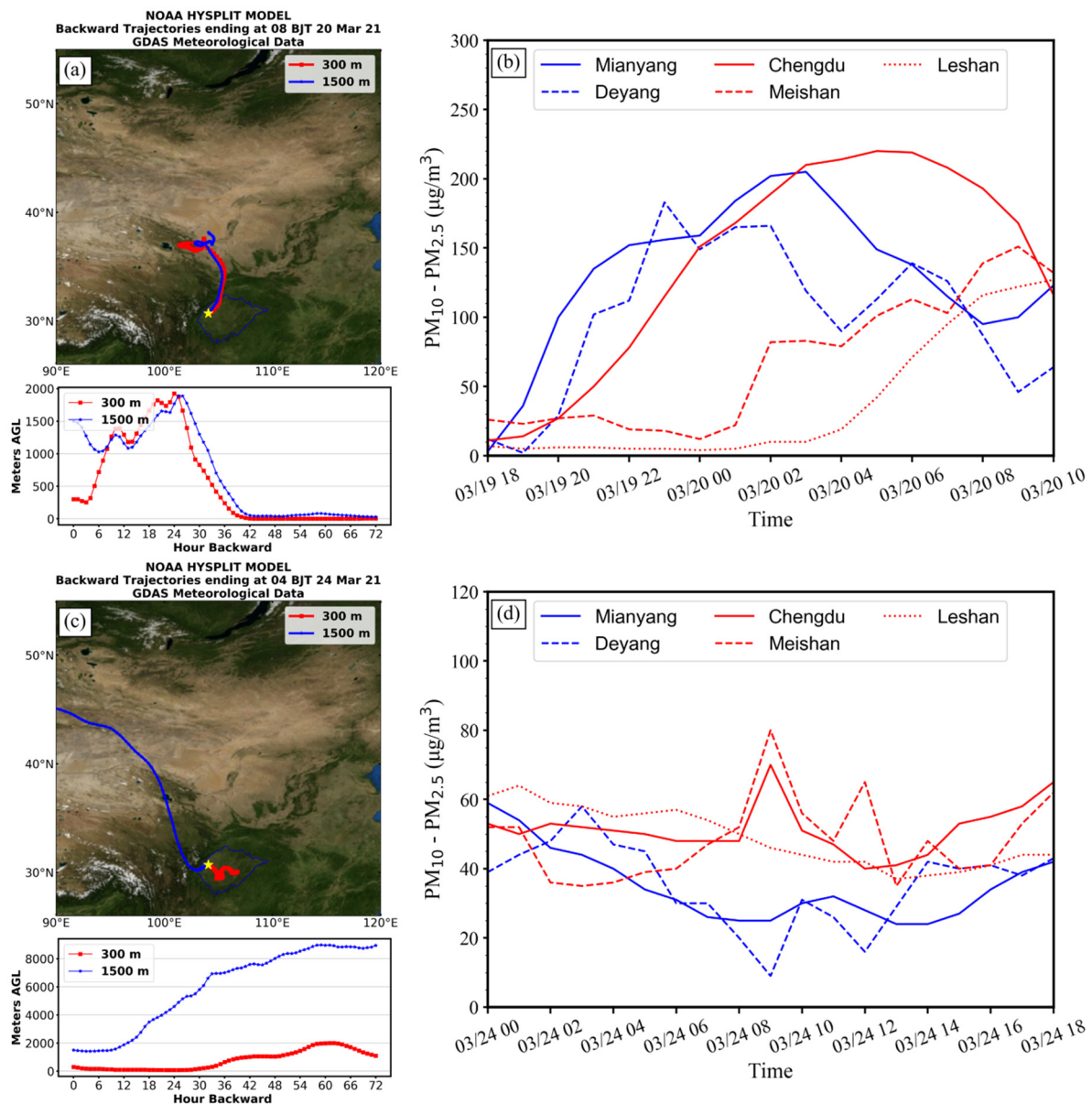
Figure 2. The 72-h backward trajectories starting at 300 m and 1500 m above ground level at 08:00 on 20 March 2021 (**a**) and 04:00 on 24 March 2021 (**c**) in Chengdu, and the concentrations of coarse particles (PM$_{10}$−PM$_{2.5}$) in Chengdu during 18:00 on 19 March and 10:00 on 20 March 2021 (**b**) and during 00:00 and 18:00 on 24 March (**d**).

3.2. Two Dust Transportation Mechanisms

Figure 3a,b shows the vertical characteristics of extinction coefficients and depolarization ratios from lidar at Chengdu from 19 March to 26 March, 2021. It could be found that Chengdu was covered by clouds during most of the dust event. Accompanied by different status of cloud cover, two mechanisms of dust transportation were identified. In the beginning of dust intrusion (around 18 p.m. BJT on 19 March), the cloud base was located at heights between 1500 m to 3500 m. Beneath the cloud layer, the extinction coefficients and depolarization ratios increased abruptly. The maximum depolarization ratio exceeded 0.3 and the highest extinction coefficients concentrated from 500 m to 1000 m above ground level. As shown in Figure S1, the concentrations of coarse particles (PM$_{10}$−PM$_{2.5}$) near the surface increased simultaneously with the extinction coefficients in the upper air. Furthermore, northerly winds prevailed in Chengdu before 20 p.m. on 20 March as shown in

Figure 3c. These results indicated that the dust particles affecting Chengdu were mainly transported into the basin in the whole layer beneath the clouds during the beginning stage of this dust event.
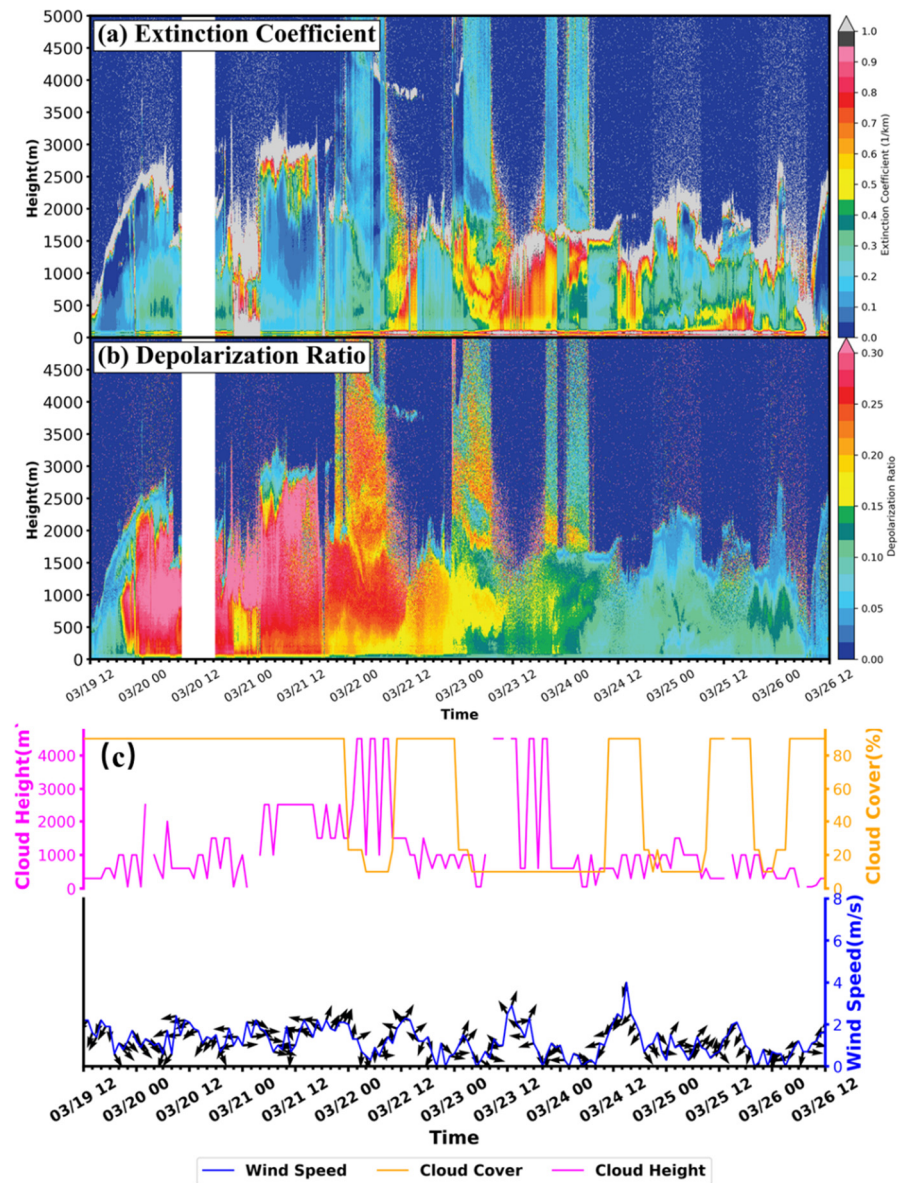

Figure 3. The extinction coefficients (**a**) and depolarization ratios (**b**) measured by ground lidar and near surface meteorological parameters (**c**) at Chengdu from 19 March to 26 March 2021.

The second mechanism occurred over cloudless areas and was characterized by settling down from upper air. As seen in Figure 3, during cloudless periods the extinction coefficients were non-negligible and depolarization ratios were greater than 0.2 in the upper air (up to 5 km above ground), which revealed that many dust particles suspended there. Along with the dissipation of clouds, these dust particles settled down without the obstruction of clouds starting at 22:00. on 21 March and 00:00 on 23 March, respectively. Correspondingly, the concentrations of near surface coarse particles increased and $PM_{2.5}/PM_{10}$ ratios decreased several hours later, as shown in Figure S1.

Once the dust particles intruded the basin through these two mechanisms, they could also be transported in the basin area. In Figure 3a,b some discrete patterns with high extinction coefficients and depolarization ratios were found, such as the results during

06:00–12:00 on 22 March and 00:00–06:00 on 24 March. Meanwhile, more southerly winds were recorded in these periods as shown in Figure 3c. Hence, it was reasonable to assume that these discrete patterns were caused by the advection of dust particles in the basin.

3.3. Typical Transportation Cases

We took the transportation processes at 18:00. on 19 March and 04:00 on 24 March as typical cases representing the first and second mechanisms, respectively. Figure 4 presents characteristics of meteorological parameters for these two cases. On 19 March, an extremely high-pressure system located to the north of the Sichuan Basin, led to strong northerly winds prevailing in the basin area. This is consistent with the trajectories presented in Figure 2. Meanwhile, the whole basin was covered by clouds with cloud bases at 1000–2000 m above ground as shown in Figure 4a. The gap between the topography and cloud bases in the northern edge of the basin allowed the northerly winds to bring dust particles into the basin (the first mechanism).
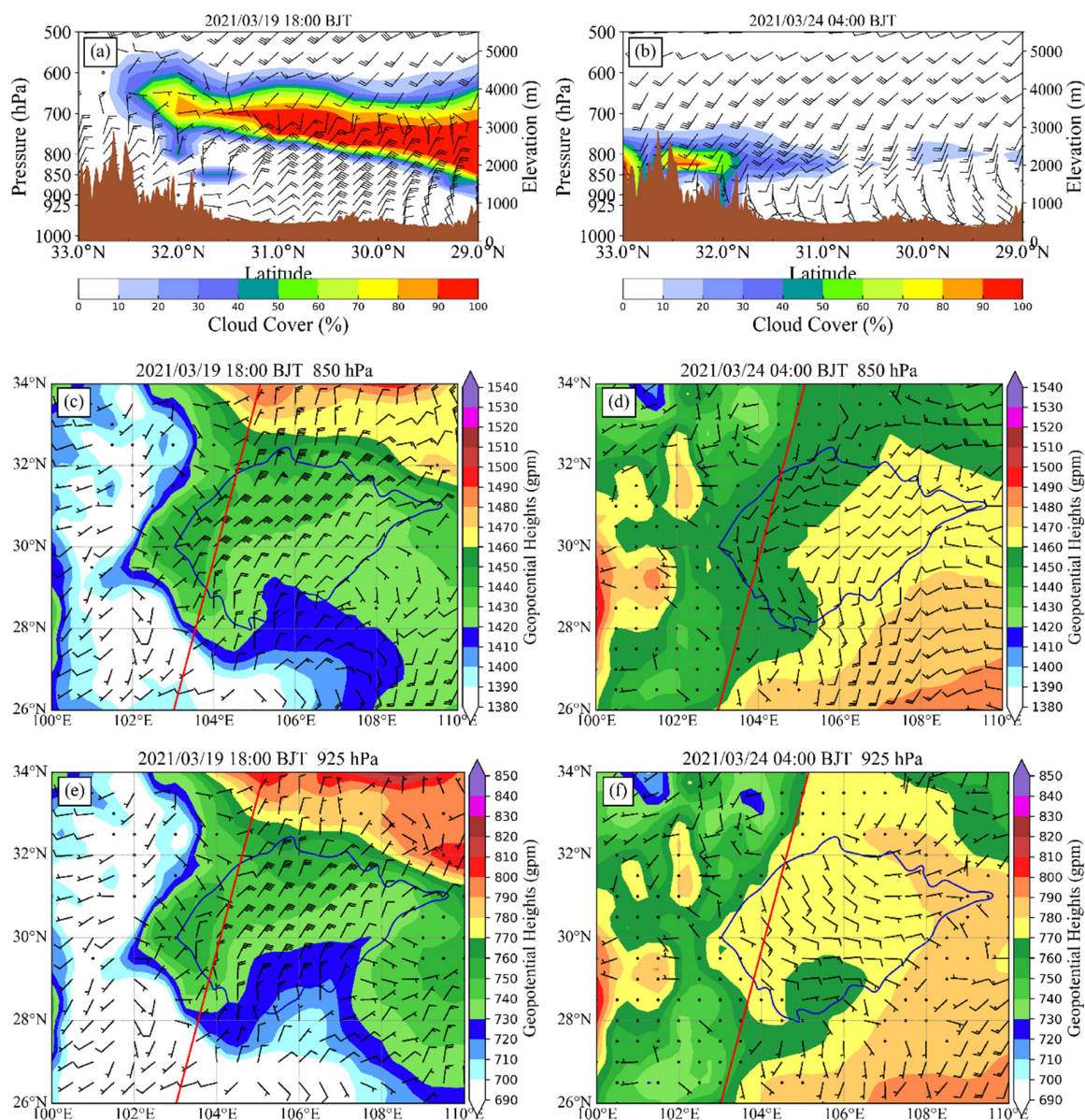

Figure 4. The cross-section of cloud fractions along the red line (**a**), the geopotential heights and horizontal wind fields at 850 hPa (**c**), and 925 hPa (**e**) at 18 p.m. BJT on 19 March 2021 from ERA5

reanalysis data. Panels (**b**,**d**) and (**f**) present the same contents as (**a**,**c**) and (**e**), respectively, but at 04:00 on 24 March 2021. The wind barbs in panels (**a**) and (**b**) were horizontal winds. Each red line presented the path of CALIPSO sub-satellite point around 03:38 BJT on 24 March 2021. On 24 March, the transportation of dust was more complex. The vertical mask features from CALIOP around 03:38 on 24 March are presented in Figure 5 to examine the dust distribution across the basin rather than at a fixed location. The clouds on the northern edge were much lower and the gap between the topography and cloud bases disappeared. In this case, although obvious dust layers located in the northern area outside the basin as shown in Figure 5, dust particles could not penetrate the cloud layers into the basin. Hence, the first transportation mechanism did not occur efficiently. In the middle and southern part of the basin, the second mechanism worked and made the whole layer up to 5 km was filled with polluted dust particles. Consequently, $PM_{2.5}/PM_{10}$ ratios in a northern city (Mianyang) were obviously higher than those in southern city (Meishan) as shown in Figure S1, and the concentration of coarse particles in a northern city were obviously lower than those in southern city, as shown in Figure 2d. Moreover, the dust particles settled down from upper air in the cloudless area might be transported to the cloudy area in lower layers. As shown in Figure 5a, Chengdu was in the connection zone between cloudy and cloudless areas. Meanwhile, the high pressure system in the north of the basin as shown in Figure 4c,e moved to the southeast of the basin (Figure 4d,f), resulting in southwesterly winds on 850 hPa (about 1000 m above ground) and southeasterly winds on 925 hPa (about 400 m above ground), respectively. This advection feature might be the cause of the observed discrete dust pattern in Figure 3a,b.
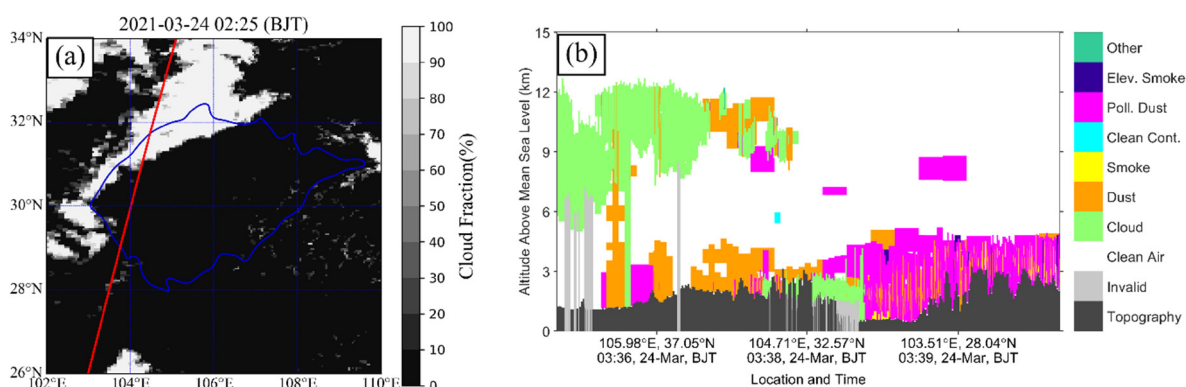

Figure 5. The distribution of MODIS Cloud fractions and the path of CALIPSO sub-satellite point (**a**) and the vertical mask features from CALIOP (**b**) around 03:38 a.m. BJT on 24 March 2021. The red line was the same as those in Figure 4.

4. Conclusions

In this study, we found that the existence of low-level clouds on the north and west edge of the basin could also prevent the dust breaking into the basin through the northern and northwestern pathways. In this case, the dust particles in the upper layer could settle down in the cloudless area and transport to other regions beneath the clouds. The Sichuan Basin was the region with the highest cloud amount in China, especially in spring [21]. In addition to the mountains around the basin, the clouds over the Sichuan Basin might be another import factor influencing the transportation of northern dust into the basin.

References

1. Kok, J.F.; Ward, D.S.; Mahowald, N.M.; Evan, A.T. Global and regional importance of the direct dust-climate feedback. *Nat. Commun.* **2018**, *9*, 241. [CrossRef]
2. Solomon, S.; Qin, D.; Manning, M.; Averyt, K.; Marquis, M. *Climate Change 2007—The Physical Science Basis: Working Group I Contribution to the Fourth Assessment Report of the IPCC*; Cambridge University Press: Cambridge, UK, 2007; Volume 4.
3. Zender, C.S.; Miller, R.; Tegen, I. Quantifying mineral dust mass budgets: Terminology, constraints, and current estimates. *Eos Trans. Am. Geophys. Union* **2004**, *85*, 509–512. [CrossRef]
4. Bishop, J.K.; Davis, R.E.; Sherman, J.T. Robotic observations of dust storm enhancement of carbon biomass in the North Pacific. *Science* **2002**, *298*, 817–821. [CrossRef] [PubMed]
5. De Longueville, F.; Hountondji, Y.-C.; Henry, S.; Ozer, P. What do we know about effects of desert dust on air quality and human health in West Africa compared to other regions? *Sci. Total Environ.* **2010**, *409*, 1–8. [CrossRef]
6. Sarkar, S.; Chauhan, A.; Kumar, R.; Singh, R.P. Impact of Deadly Dust Storms (May 2018) on Air Quality, Meteorological, and Atmospheric Parameters Over the Northern Parts of India. *Geohealth* **2019**, *3*, 67–80. [CrossRef] [PubMed]
7. Goudie, A.S. Desert dust and human health disorders. *Environ. Int.* **2014**, *63*, 101–113. [CrossRef]
8. Karanasiou, A.; Moreno, N.; Moreno, T.; Viana, M.; de Leeuw, F.; Querol, X. Health effects from Sahara dust episodes in Europe: Literature review and research gaps. *Environ. Int.* **2012**, *47*, 107–114. [CrossRef]
9. Huang, J.; Lin, B.; Minnis, P.; Wang, T.; Wang, X.; Hu, Y.; Yi, Y.; Ayers, J.K. Satellite-based assessment of possible dust aerosols semi-direct effect on cloud water path over East Asia. *Geophys. Res. Lett.* **2006**, *33*, L19802. [CrossRef]
10. Matsuki, A.; Schwarzenboeck, A.; Venzac, H.; Laj, P.; Crumeyrolle, S.; Gomes, L. Effect of surface reaction on the cloud nucleating properties of mineral dust: AMMA aircraft campaign in summer 2006. *Atmos. Chem. Phys. Discuss.* **2009**, *9*, 1797–1830. [CrossRef]
11. Slingo, A.; Ackerman, T.P.; Allan, R.P.; Kassianov, E.I.; McFarlane, S.A.; Robinson, G.J.; Barnard, J.C.; Miller, M.A.; Harries, J.E.; Russell, J.E.; et al. Observations of the impact of a major Saharan dust storm on the atmospheric radiation balance. *Geophys. Res. Lett.* **2006**, *33*, L24817. [CrossRef]
12. Dentener, F.J.; Carmichael, G.R.; Zhang, Y.; Lelieveld, J.; Crutzen, P.J. Role of mineral aerosol as a reactive surface in the global troposphere. *J. Geophys. Res. Atmos.* **1996**, *101*, 22869–22889. [CrossRef]
13. Groß, S.; Tesche, M.; Freudenthaler, V.; Toledano, C.; Wiegner, M.; Ansmann, A.; Althausen, D.; Seefeldner, M. Characterization of Saharan dust, marine aerosols and mixtures of biomass-burning aerosols and dust by means of multi-wavelength depolarization and Raman lidar measurements during SAMUM 2. *Tellus B Chem. Phys. Meteorol.* **2011**, *63*, 706–724. [CrossRef]
14. Chen, Y.; Luo, B.; Xie, S.-d. Characteristics of the long-range transport dust events in Chengdu, Southwest China. *Atmos. Environ.* **2015**, *122*, 713–722. [CrossRef]
15. Li, R.; Gong, J.; Zhou, J.; Sun, W.; Ibrahim, A.N. Multi-satellite observation of an intense dust event over southwestern China. *Aerosol Air Qual. Res.* **2015**, *15*, 263–270. [CrossRef]
16. Lian, J.; Wang, S.; Luo, B.; Zhang, W.; Yunsong, D.U.; Jiang, W. A Study on Regional Air Heavy Pollution Process with Double Impact of Local Emission and Dust Transport in Sichuan Basin. *Desert Oasis Meteorol.* **2019**, *13*, 122–131.

17. Tao, J.; Zhang, L.; Engling, G.; Zhang, R.; Yang, Y.; Cao, J.; Zhu, C.; Wang, Q.; Luo, L. Chemical composition of PM2. 5 in an urban environment in Chengdu, China: Importance of springtime dust storms and biomass burning. *Atmos. Res.* **2013**, *122*, 270–283. [CrossRef]
18. Zhao, Q.; He, K.; Rahn, K.A.; Ma, Y.; Jia, Y.; Yang, F.; Duan, F.; Lei, Y.; Chen, G.; Cheng, Y.; et al. Dust storms come to Central and Southwestern China, too: Implications from a major dust event in Chongqing. *Atmos. Chem. Phys.* **2010**, *10*, 2615–2630. [CrossRef]
19. Yu, R.C.; Wang, B.; Zhou, T.J. Climate effects of the deep continental stratus clouds generated by the Tibetan Plateau. *J. Clim.* **2004**, *17*, 2702–2713. [CrossRef]
20. Jia, B.; Xie, Z.; Dai, A.; Shi, C.; Chen, F. Evaluation of satellite and reanalysis products of downward surface solar radiation over East Asia: Spatial and seasonal variations. *J. Geophys. Res. Atmos.* **2013**, *118*, 3431–3446. [CrossRef]
21. Li, Y.; Yu, R.; Xu, Y.; Zhang, X. Spatial distribution and seasonal variation of cloud over China based on ISCCP data and surface observations. *J. Meteorol. Soc. Japan Ser. II* **2004**, *82*, 761–773. [CrossRef]
22. Nishizawa, T.; Okamoto, H.; Sugimoto, N.; Matsui, I.; Shimizu, A.; Aoki, K. An algorithm that retrieves aerosol properties from dual-wavelength polarized lidar measurements. *J. Geophys. Res. Atmos.* **2007**, *112*, D06212. [CrossRef]
23. He, Y.; Xu, X.; Gu, Z.; Chen, X.; Li, Y.; Fan, S. Vertical distribution characteristics of aerosol particles over the Guanzhong Plain. *Atmos. Environ.* **2021**, *255*, 118444. [CrossRef]
24. Papayannis, A.; Amiridis, V.; Mona, L.; Tsaknakis, G.; Balis, D.; Bösenberg, J.; Chaikovski, A.; de Tomasi, F.; Grigorov, I.; Mattis, I.; et al. Systematic lidar observations of Saharan dust over Europe in the frame of EARLINET (2000–2002). *J. Geophys. Res. Atmos.* **2008**, *113*, D10204. [CrossRef]
25. Sakai, T.; Nagai, T.; Zaizen, Y.; Mano, Y. Backscattering linear depolarization ratio measurements of mineral, sea-salt, and ammonium sulfate particles simulated in a laboratory chamber. *Appl. Opt.* **2010**, *49*, 4441–4449. [CrossRef]
26. Hervig, M.; McHugh, M. Cirrus detection using HALOE measurements. *Geophys. Res. Lett.* **1999**, *26*, 719–722. [CrossRef]
27. Pinnick, R.; Jennings, S.; Chýlek, P.; Ham, C.; Grandy, W., Jr. Backscatter and extinction in water clouds. *J. Geophys. Res. Ocean.* **1983**, *88*, 6787–6796. [CrossRef]
28. Winker, D.M.; Hunt, W.H.; McGill, M.J. Initial performance assessment of CALIOP. *Geophys. Res. Lett.* **2007**, *34*, L19803. [CrossRef]
29. Yang, W.; Marshak, A.; Varnai, T.; Kalashnikova, O.V.; Kostinski, A.B. CALIPSO observations of transatlantic dust: Vertical stratification and effect of clouds. *Atmos. Chem. Phys.* **2012**, *12*, 11339–11354. [CrossRef]
30. Platnick, S.; King, M.D.; Ackerman, S.A.; Menzel, W.P.; Baum, B.A.; Riédi, J.C.; Frey, R.A. The MODIS cloud products: Algorithms and examples from Terra. *IEEE Trans. Geosci. Remote Sens.* **2003**, *41*, 459–473. [CrossRef]
31. Platnick, S.; Meyer, K.G.; King, M.D.; Wind, G.; Amarasinghe, N.; Marchant, B.; Arnold, G.T.; Zhang, Z.; Hubanks, P.A.; Holz, R.E. The MODIS cloud optical and microphysical products: Collection 6 updates and examples from Terra and Aqua. *IEEE Trans. Geosci. Remote Sens.* **2016**, *55*, 502–525. [CrossRef] [PubMed]
32. Hersbach, H.; Bell, B.; Berrisford, P.; Biavati, G.; Horányi, A.; Muñoz Sabater, J.; Nicolas, J.; Peubey, C.; Radu, R.; Rozum, I. ERA5 Hourly Data on Pressure Levels from 1979 to Present. In Copernicus Climate Change Service (c3s) Climate Data Store (cds). 2018. 10. Available online: http://doi.org/10.24381/cds.bd0915c6 (accessed on 7 June 2021). [CrossRef]
33. Draxier, R.R.; Hess, G.D. An overview of the HYSPLIT_4 modeling system of trajectories, dispersion, and deposition. *Aust. Meteorol. Mag.* **1998**, *47*, 295–308.
34. Liu, B.; Peng, W.; Liu, S.; Yang, T. Estimation on the dust lift amount and source contribution of the heavy dust weather in mid-March 2021 over Central East Asia. *J. Desert Res.* **2022**, *42*, 79.
35. Yin, Z.; Wan, Y.; Zhang, Y.; Wang, H. Why super sandstorm 2021 in North China? *Natl. Sci. Rev.* **2022**, *9*, nwab165. [CrossRef] [PubMed]
36. Nasa/Larc/Sd/Asdc. CALIPSO Lidar Level 2 Vertical Feature Mask (VFM), V4-20. Available online: https://doi.org/10.5067/CALIOP/CALIPSO/LID_L2_VFM-STANDARD-V4-20 (accessed on 30 August 2021).
37. Platnick, S.; Ackerman, S.; King, M.; Meyer, K.; Menzel, W.; Holz, R.; Baum, B.; Yang, P. MODIS atmosphere L2 cloud product (06_L2). *NASA MODIS Adapt. Process. Syst. Goddard Space Flight Cent.* **2015**, *10*, 1–53. Available online: http://doi.org/10.5067/MODIS/MYD06_L2.006 (accessed on 30 August 2021).